

Relaxation to Equilibrium in a Quantum Network

J. Novotný,¹ A. Mariano,² S. Pascazio,^{3,4} A. Scardicchio,^{5,6} and I. Jex¹

¹*Department of Physics, Czech Technical University in Prague, 115 19 Praha 1 - Staré Město, Czech Republic*

²*ENEA, Italian National Agency for New Technologies, Energy,
and Sustainable Economic Development, via G. Petroni 15/F, I-70124 Bari, Italy*

³*Dipartimento di Fisica and MECENAS, Università di Bari, I-70126 Bari, Italy*

⁴*INFN, Sezione di Bari, I-70126 Bari, Italy*

⁵*The Abdus Salam International Center for Theoretical Physics, Strada Costiera 11, 34151 Trieste, Italy*

⁶*INFN Sezione di Trieste, I-34127 Trieste, Italy*

The approach to equilibrium of quantum mechanical systems is a topic as old as quantum mechanics itself, but has recently seen a surge of interest due to applications in quantum technologies, including, but not limited to, quantum computation and sensing. The mechanisms by which a quantum system approaches its long-time, limiting stationary state are fascinating and, sometimes, quite different from their classical counterparts. In this respect, quantum networks represent a mesoscopic quantum systems of interest. In such a case, the graph encodes the elementary quantum systems (say qubits) at its vertices, while the links define the interactions between them. We study here the relaxation to equilibrium for a fully connected quantum network with CNOT gates representing the interaction between the constituting qubits. We give a number of results for the equilibration in these systems, including analytic estimates. The results are checked using numerical methods for systems with up to 15-16 qubits. It is emphasized in which way the size of the network controls the convergence.

PACS numbers:

I. INTRODUCTION

Quantum networks [1, 2] find a wide range of applications in quantum theory and information processing. In rather general terms, a quantum network is an ensemble of quantum systems—typically qubits—with a prescribed set of interactions between them, defining the overall pattern that enables them to carry out specific tasks. Quantum networks can have different degrees of complexity and hence also execute tasks that can be more or less sophisticated. Quantum networks can be used to carry out computations, communications or storage of quantum information [3, 4].

The information about the details of the network and the mutual interactions between its constituting parts is efficiently encoded into graphs. The vertices represent the quantum systems and the edges (links) the interactions between the network elements. In the simplest case the links of the graph are static and unchangeable. In such a case we assume that the network dynamics is described by a unitary dynamics which is not changing in time. However, it is not difficult to generalize such a structure to encompass more general situations. The links between the elements of the network can be activated or terminated and the underlying graph encodes then only the potentiality of two or more elements to interact. Such situations can describe, for instance, a quantum gas where the elements of the network are not qubits but atoms or molecules and by using the concept of network we follow the formation of the asymptotic-stationary states due to elementary interactions between them [5, 6]. In such a case each link-edge is given a weight representing the probability with which a given

interaction is carried out and hence we follow the evolution of the system with sufficient time resolution. Such a situation is inherently random and while the elementary time evolution (represented by a given sequence of operations) is unitary and given by the product of individual unitary operations, the overall evolution is non-unitary [7]. Even though all input states are available, the evolution of the system tends in general to an attractor space of the network and does not take place in a subspace of the original Hilbert space. The evolution of the system is described by the repeated application of a completely positive map. The basic task in solving the dynamics of the network is twofold: one first determines the asymptotic space, and then finds the rate at which the system approaches this subspace. Such a task is in general intimately linked to the choice of the graph chosen, the weight of the links and naturally the form of interaction between the constituting parts. In the following we will focus on qubit networks with CNOT operations between any chosen pair of qubits, hence the underlying graph will be the fully connected graph [8, 9].

These collision models are reminiscent of the popular Boltzmann gas model of statistical physics [5, 10, 11], in which one has sufficient time resolution to guarantee that only bipartite interactions be considered. Models of this type are routinely used in the study of the approach to equilibrium, transport phenomena, decoherence and dephasing, and the study of temporal synchronization [12]. In this context, it is worth of notice that the approach to equilibrium, and lack thereof, of a quantum system has received a lot of attention due to both theoretical advances [13–22] and experimental results [23, 24]. More to our problem, one can imagine that, with the advent of the first digital quantum computers [25], the dynamics

of quantum networks could be experimentally simulated, and, conversely, will have bearing on the behavior of running quantum algorithms. In particular, one has in mind population transfer and similar algorithms [26–28] which can benefit from fast development of ergodicity over a subset of preferred configurations (the equilibration time is the running time of the algorithm).

One of the fundamental aspects of quantum networks is the presence, creation and transmission of entanglement. For qubits entanglement can be formed in different ways and one of them is the use of CNOT operations between them. When such operations are applied in networks the CNOT operations compete against each other in entanglement formation (monogamy of two-particle entanglement) and the asymptotic regime (state) of the network is a density matrix of a rather simple form. The process can also be viewed as a competition between entanglement creation among the qubits and decoherence originating from the imperfect control over the system.

While the determination of the asymptotic regime is given by the solution of a well-defined set of conditions specified by the underlying graph structure (and independent of the actual weights of the edges), the rates of convergence to the asymptotic is crucially dependent of these weight. The structure of the asymptotic state is quite clear and even accessible to analytic treatment; on the other hand, the question of the convergence rates is largely unexplored and depends on a much larger set of parameters than the structure of the asymptotic space.

In the following we provide quantitative estimates for the convergence of a fully connected graph undergoing CNOT interactions. This simple example enables us both to demonstrate the influence of the network size (number of qubits) on the convergence rate at leading order, and discuss the influence of the geometry of the network, focusing in particular on two limiting cases, the complete graph and the circle graph. We shall also give a few hints on the influence of altering the edge probability (via the introduction of noise) on the convergency rate. A full understanding of our numerical outcomes will be obtained in the light of a general theorem on the convergency rate.

The properties to be discussed in the following sections make CNOT gates particularly appealing on a number of grounds. First of all, they are entanglement forming (although, as discussed before, the map will induce dephasing, adding an inherent competition in the global dynamics); second, they are mathematically simple, and in particular they form a finite group (see Secs. III and IV); third, propagation and/or entanglement loss in an n -partite system are of general interest for the quantum information community; finally, CNOT is a special case of controlled rotations, which are the building blocks of dephasing in collisional models [8].

This article is organized as follows. We set up the problem and introduce notation in Sec. II. In Sec. III we make an observation that leads to a drastic simplification of the problem. In Sec. IV we clarify the general framework in terms of a rather elementary example that

can be solved explicitly. The problem is then recast in simpler terms in Sec. V. We perform a numerical analysis in Sec. VI, and conclude in Sec. VII.

II. SETTING UP THE PROBLEM

We consider N qubits with the Hilbert space $\mathcal{H} = (\mathbb{C}^2)^{\otimes N}$ undergoing the following iterated dynamical evolution [7, 8]

$$\Phi(\rho) = \sum_{i \in I} p_i U_i \rho U_i^\dagger, \quad (1)$$

where state $\rho \in \mathcal{T}(\mathcal{H})$ is a trace class operator on the Hilbert space \mathcal{H} , U_i are unitaries, p_i a probability distribution and I a set of indices (each representing a couple of qubits). We shall focus on the behavior of the iterated map $\Phi^n(\rho) = \Phi(\Phi(\dots(\Phi(\rho))))$ and its speed of convergence to equilibrium when the U_i 's are CNOT gates, acting on qubits a and b according to

$$U_{i=(a,b)} = \text{CNOT}_{(a,b)} \otimes \mathbf{1}_{\text{rest}}, \quad (2)$$

and the interaction graph is fully connected. However, some of the ideas presented here are valid for more general networks and will be presented elsewhere.

We first observe that the superoperator (1) is linear, so that its eigenvalues are Lyapunov coefficients. Moreover, it is also normal, so that it admits an orthonormal set of attractors, spanning a linear manifold Π , and an additional orthonormal set corresponding to eigenvalues $|\beta| < 1$, the two sets making up a basis. Let $\rho(n) = \Phi^n(\rho(0))$ be the state after n -th iteration. Employing a Hilbert-Schmidt distance $d(\rho_1, \rho_2) = \|\rho_1 - \rho_2\| = [\text{Tr}(\rho_1 - \rho_2)^2]^{1/2}$ one can prove that

$$d(\rho(n), \Pi) \leq (\beta_*)^n d(\rho(0), \Pi), \quad (3)$$

where $\beta_* = \max_{|\beta| < 1} |\beta|$ denotes the maximal absolute value of the eigenvalues $|\beta| < 1$ and is known as the *subleading* eigenvalue of the map [29, 30]. Hence, the speed of convergence to equilibrium is bounded by the subleading eigenvalue β_* . A concrete example is shown in Fig. 1: one notices that the dynamics significantly depends on the initial state and the bound (3) appears to be rather loose.

The aim of this article is to analyze the rate of convergence for (rather large) networks. This is a difficult problem, because it involves the eigenvalue of large superoperators (e.g., for as few as 20 qubits the dimension of the superoperator is $2^{40} \simeq 10^{12}$) and depends on the rich structure of the interaction graphs. We shall therefore look for upper bounds of the subleading eigenvalue.

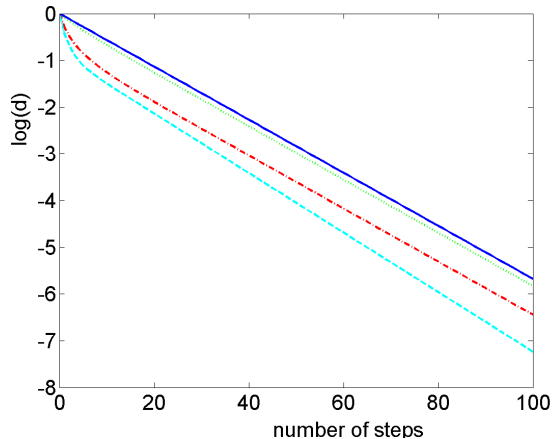


FIG. 1: Distance d in Eq. (3) between evolving states and their corresponding asymptotic limits: We considered a fully connected network of 6 qubits with equally distributed weights. The (blue) solid line represents the upper bound in Eq. (3). The (green) dotted, (red) dash-dotted and (light-blue) dashed lines correspond to initial states $|000001\rangle, |101010\rangle, |111111\rangle$, respectively.

III. A PRELIMINARY OBSERVATION

We start from an observation. Consider the random unitary channel (1)

$$\Phi(\cdot) = \sum_{i \in I} p_i U_i(\cdot) U_i^\dagger \quad (4)$$

and let $|e_i\rangle$ be an orthonormal basis of the Hilbert space \mathcal{H} . This map acts on the matrices ρ . In the basis $|e_i\rangle\langle e_j|$, since

$$\begin{aligned} \text{Tr}(|e_b\rangle\langle e_a| \Phi(|e_i\rangle\langle e_j|)) &= \langle e_a | \Phi(|e_i\rangle\langle e_j|) | e_b \rangle \\ &= \sum_{i \in I} p_i \langle e_a | U_i | e_i \rangle \langle \langle e_b | U | e_j \rangle \rangle^* \end{aligned} \quad (5)$$

the matrix form of map Φ reads

$$\Phi = \sum_{i \in I} p_i U_i \otimes U_i^*, \quad (6)$$

where $*$ means complex conjugation. For the particular case (2) (CNOT gates, on which we shall focus)

$$U_i = U_i^\dagger = U_i^*, \quad \text{and so} \quad U_i^2 = 1, \quad (7)$$

and we are therefore interested in the eigenvalues of the map

$$\Phi = \sum_{i \in I} p_i U_i \otimes U_i. \quad (8)$$

Consider the operators $\mathcal{U}_i = U_i \otimes U_i$ on the space $\mathcal{H} \otimes \mathcal{H}$. Notice that the group properties of \mathcal{U}_i and U_i are

exactly the same: $\mathcal{U}_i^2 = 1$, while algebraic properties are not necessarily maintained, e.g. an equation $U_i U_j = a U_k$ would map to $\mathcal{U}_i \mathcal{U}_j = a^2 \mathcal{U}_k$. However, for CNOT gates these equations never generate coefficients $a \neq 1$, so the full algebraic properties are maintained.

Notice also that Φ can be viewed as the average of the random process

$$F = \mathcal{U}_i, \quad \text{with probability } p_i, \quad (9)$$

in the sense that

$$\Phi = \langle F \rangle. \quad (10)$$

Moreover, using the superoperator space trace,

$$\text{Tr} \Phi = \text{Tr} \langle F \rangle = \langle \text{Tr} F \rangle, \quad (11)$$

and higher traces are connected to the multiplicative random process (MRP)

$$\text{Tr} \Phi^n = \text{Tr} \left\langle \prod_{a=1}^n F_a \right\rangle, \quad (12)$$

where F_a are independent F random variables. This is due irrespective of the definition of Tr but only to its linearity.

Using now that fact that for CNOT gates $\mathcal{U}_i \sim U_i$ is an algebra-preserving isomorphism, it is not difficult to convince oneself that we obtain, for purpose of computing $\text{Tr}(\Phi^n)$ and therefore the maximum Lyapunov exponent, a completely equivalent problem if we simplify the situation and consider the map

$$\phi = \sum_{i \in I} p_i U_i \quad (13)$$

and the random process

$$f = U_i \quad \text{with prob. } p_i, \quad (14)$$

with associated MRP. The usual definition of operator trace is used. Notice that some quantitative features comparing F and f are lost, since the values of the superoperator and operator traces are different. This gives rise to different spectra, although the important eigenvalues (the largest and second largest) are the same in all cases we have analyzed.

Let us now concentrate on the case of f and let G be the multiplicative group generated by the operators U_i . We write $G = \{g_a\}_{a=1, \dots, M}$ and $1, U_i \in G$. In the case of the CNOT gates to be considered in this article, this group is a finite subgroup of the (finite) group $GL_n(\mathbf{F}_q)$. Then

$$\text{Tr} \phi^n = \sum_a k_a(n) \text{Tr}(g_a), \quad (15)$$

where $k_a(n)$ are coefficients measuring the probability that the MRP starting at $n = 0$ in the identity, ends

up in g_a after n steps. The MRP on the group is represented by a M -by- M matrix $W_{a,b}$. The matrix is real and stochastic. Assuming it is also symmetric we can solve this problem using eigenvalues ω_a and eigenvectors $|\omega_a\rangle$ of the matrix W

$$k_a(n) = \sum_{b=1,\dots,M} \omega_b^n \langle g_a | \omega_b \rangle \langle \omega_b | 1 \rangle, \quad (16)$$

where $|1\rangle$ is the vector associated with the group element identity $g_a = 1$.

IV. AN EXAMPLE

Let us look at an explicit example. Consider the case of two qubits with $p_1 = p$ and $p_2 = 1 - p$. The group $G = \{1, U_1, U_2, U_1 U_2, U_2 U_1, U_1 U_2 U_1 = U_2 U_1 U_2\}$. The matrix representing the MRP is

$$W = \begin{pmatrix} 0 & p & 1-p & 0 & 0 & 0 \\ p & 0 & 0 & 0 & 1-p & 0 \\ 1-p & 0 & 0 & p & 0 & 0 \\ 0 & 0 & p & 0 & 0 & 1-p \\ 0 & 1-p & 0 & 0 & 0 & p \\ 0 & 0 & 0 & 1-p & p & 0 \end{pmatrix}, \quad (17)$$

with eigenvalues

$$\omega_a = \left(1, -1, -\sqrt{1-3p+3p^2}, -\sqrt{1-3p+3p^2}, \sqrt{1-3p+3p^2}, \sqrt{1-3p+3p^2} \right). \quad (18)$$

The Perron-Frobenius theorem [31], together with stochasticity, guarantees that the maximum eigenvalue is 1 and corresponds to the uniform eigenvector

$$\langle g_a | \omega_1 \rangle = \frac{1}{\sqrt{6}}. \quad (19)$$

The eigenvector corresponding to eigenvalue -1 is

$$\langle g_a | \omega_2 \rangle = \frac{(-1)^{P_a}}{\sqrt{6}}. \quad (20)$$

where P_a is the parity of g_a , which is 0 for $1, U_1 U_2, U_2 U_1$ and -1 for the remaining 3 elements. The remaining subleading eigenvalues $s = \pm\sqrt{1-3p+3p^2}$ with their associated eigenvectors $|s_c\rangle_{c=1,\dots,4}$. Notice that the subleading eigenvalue coincides with that obtained by explicit calculation. Putting all together we find

$$\text{Tr } \phi^n = \frac{1}{6} 1^n \sum_a \text{Tr}(g_a) + \frac{1}{6} (-1)^n \sum_a (-1)^{P_a} \text{Tr}(g_a) + s^n A. \quad (21)$$

Notice that

$$\sum_a \text{Tr}(g_a) = 12, \quad (22)$$

$$\sum_a (-1)^{P_a} \text{Tr}(g_a) = 4 + 1 + 1 - 2 - 2 - 2 = 0, \quad (23)$$

so that

$$\text{Tr } \phi^n = 2 + s^n A, \quad (24)$$

which means that the leading and sub-leading eigenvalues of ϕ are given by the leading and sub-leading eigenvalues of W . Notice how the $\text{Tr}(g_a)$ is reflected in the degeneracy of the eigenvalues (for example 2 for the eigenvalue 1).

The only non-trivial step is the cancellation of the contribution of the eigenvalue -1 . It is not difficult to prove that i) this eigenvalue always exists and it is due to the fact that parity breaks the group G in two, G_+ and G_- and that the MRP necessarily connects $G_{\pm} \rightarrow G_{\mp}$, and ii) that its contribution, once the trace is taken, is always 0. Therefore, we can assert that the sub-leading eigenvalue of W is the sub-leading eigenvalue of ϕ .

We now go back to the problem of the map Φ . One can repeat exactly the same steps as before if we identify the group G as generated by $U_1 \otimes U_1$ and $U_2 \otimes U_2$. This is exactly the same group G as before (it is the diagonal projection of the group $G \otimes G$) and therefore the very same calculations occur. There is one, crucial difference as the superoperator trace Tr will give different results from the operator trace Tr . This affects the polynomials $\text{Tr } \phi^n$ and $\text{Tr } \Phi^n$ but we observe that this *does not change the subleading eigenvalue* which is the same in both maps in all the examples we have checked. Therefore, the rate to approach to ergodicity is the same for both maps.

V. A SIMPLER PROBLEM AND SOME BOUNDS

The observation in Sec. III and the explicit example in Sec. IV show that the eigenvalue problem can be significantly simplified for certain types of interaction graphs and unitaries. Consider the random unitary channel Φ in Eq. (1) and let $\sigma(\Phi)$ be the spectrum of Φ and $\sigma_1(\Phi)$ the set of the elements of $\sigma(\Phi)$ with magnitude one. Consider now the operator

$$\phi = \sum_{i \in I} p_i U_i. \quad (25)$$

Then for certain quantum networks the subleading eigenvalue of the operator (6) coincides with the subleading eigenvalue of the operator (25) and both are positive, i.e.

$$\beta_*(\Phi) = \sup_{\lambda \in \sigma(\Phi) \setminus \sigma_1(\Phi)} \lambda = \beta_*(\phi) = \sup_{\lambda \in \sigma(\phi) \setminus \sigma_1(\phi)} \lambda. \quad (26)$$

This property has been numerically checked and appears to be valid for a wide class of *fully connected* graphs (made up of e.g., unitary transpositions, controlled and/or local rotations and the special case of CNOT gates analyzed in this article). On the other hand, it is not valid for general (e.g., non fully connected) graphs. We shall assume henceforth that the property is

valid, at least in the cases to be investigated in this article.

We now turn to the study of the specific features of the subleading eigenvalue of operator (25) when all unitaries U_i are CNOT gates acting on two qubits only, as in (1)-(2), and leaving the remaining ones unchanged. In such a case, in the computational basis, operator (25) is bistochastic or doubly stochastic

$$\sum_{i=1}^{2^N} \phi_{ij} = \sum_{j=1}^{2^N} \phi_{ij} = 1, \quad \forall 1 \leq i, j \leq 2^N \quad (27)$$

and is the adjacency matrix of an undirected weighted graph G , whose vertices are elements of the computational base and where there is an edge between two vertices (basis vectors) whenever one vector is the image of the second one under application of some U_i . Due to this definition the graph can contain loops. The weight of an edge is the sum of the probabilities assigned to the unitary operations that define this edge. In other words, a unitary operator U_i contributes to the weight of an edge with probability p_i if the vectors corresponding to the end vertices of the edge are images of each other under application of this U_i (edges are not directed, as $\text{CNOT}^2 = \mathbb{1}$). This definition applies also for loops. As a simple consequence, the weights of the edges adjacent to a given vertex, with the inclusion of the weights of loops, always sum up to one. Now, the operator ϕ is simply the adjacency matrix of this weighted graph G . Because the interaction graph is fully connected, the graph G has two components of continuity: the vertex corresponding to the vector with zero excitation and the remaining connected vertices. The one-vertex component contributes to the spectrum of Laplacian matrix by one zero eigenvalue. Let us remove this vertex from the graph in order to still have a connected graph G_ϕ with its adjacency matrix A_ϕ and its Laplacian matrix given by [32, 33]

$$L_\phi = \mathbb{1} - A_\phi, \quad (28)$$

where $\mathbb{1}$ is the $(2^N - 1) \times (2^N - 1)$ identity matrix. Equation (28) follows from the fact that the degree of each vertex is one. An example of such a graph G_ϕ is displayed in Fig. 2. The interaction graph is the 3-qubit oriented star. Only edges contributing to the weights of a given edge are explicitly displayed. Loops are not displayed.

Let us denote the algebraic connectivity [34] (the second-smallest eigenvalue (counting multiple eigenvalues separately) of the Laplacian matrix of G) of the graph G_ϕ by γ_ϕ . From the previous discussion it follows that

$$\beta_*(\Phi) = \beta_*(\phi) = 1 - \gamma_\phi \quad (29)$$

Hence, spectral graph theory can be employed to find a good lower bound for the algebraic connectivity and use it to upper bound the subleading eigenvalue of the superoperator Φ .

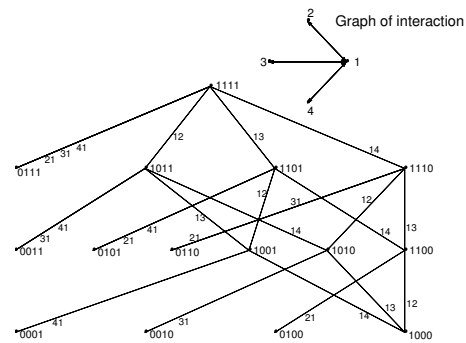


FIG. 2: Graph G_ϕ induced by graph of interaction: 4-qubit oriented star. Vertices correspond to elements of computational basis. Two vertices are linked iff one of them is an image of the other under some CNOT gate from the interaction graph. The list of pairs of indices are the CNOT gates which contribute to weights of a given edge.

In order to obtain meaningful bounds, let us start by noting that

$$\gamma_\phi \geq \frac{4}{(2^N - 1)\text{diam}(G_\phi)}, \quad (30)$$

“diam” being the diameter of the graph. This is easy to prove [36]. This bound has the advantage of being valid for an arbitrary interaction graph with an arbitrary probability distribution. The disadvantage is that it exponentially depends on the number N of qubits. Of course, this simply recasts the problem in terms of determining the diameter of the (weighted or unweighted) graph G_ϕ (which is possible at least in particular cases). For example, for a circle unweighted interaction graph with N vertices, the associated graph G_ϕ has $\text{diam}(G_\phi) = 2(N - 1)$, while for a fully connected unweighted graph with N vertices, the associated graph G_ϕ has $\text{diam}(G_\phi) = N$. The diameter of weighted graphs are much more involved.

As shown Fig. 2, the vertices corresponding to the same number of excitations are not connected. They can be connected only to vertices whose number of excitation differ by one [37].

In the case we are considering (fully connected interaction graph with random CNOT gates acting on pairs of qubits), two vertices of the graph G_ϕ are connected if and only if their excitations differ only for one qubit. Therefore, omitting the weights of the graph G_ϕ , the associated unweighted graph G'_ϕ is almost the hypercube H_n , the only difference being that the graph G'_ϕ does not contain the vertex $|0, 0, \dots, 0\rangle$ and its adjacent edges. As a consequence [34], $\gamma'_\phi \geq \gamma_{H_n} - 1 = 2 - 1 = 1$ and therefore

$$\gamma_\phi \geq \min_{ij \in I} p_{ij}. \quad (31)$$

This is the bound shown in Fig. 1: it depends very weakly on the weights, but does not depend exponentially on the number of qubits, which makes it useful. A relevant

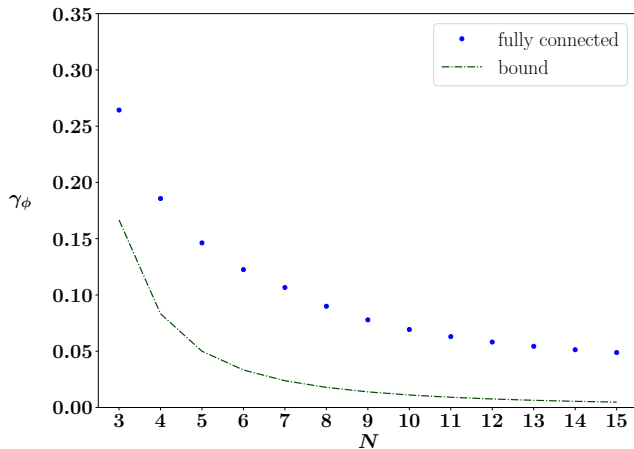


FIG. 3: Fully connected graph with equally distributed weights. Dots: algebraic connectivity. Dash-dotted (green) line: bound (31).

situation is when the probabilities are equally distributed on the N (fully connected) qubits

$$p_{ij} = \frac{1}{N(N-1)}, \quad \forall i, j. \quad (32)$$

VI. NUMERICAL ANALYSIS

We now turn to a numerical analysis. The analysis has been performed on the CRESCO/ENEAGRID High Performance Computing infrastructure [35]. The numerical evaluations have been performed on the “small” map ϕ in Eq. (13), for fully connected graphs of CNOT gates (2). In the light of our discussion, the results are also valid for the “larger” map Φ in Eq. (1). For the sake of comparison, we also performed some analyses for interaction *circle* graphs of CNOT gates.

Figure 3 displays the algebraic connectivity γ_ϕ of a fully connected graph with equally distributed weights, as in (32), for $3 \leq N \leq 15$. The bound (31) is shown for comparison and appears to be far from tight. The approach to equilibrium, measured by the subleading eigenvalue of the superoperator Φ , $\beta_*(\Phi) = \beta_*(\phi)$ in Eq. (29), is slower for increasing N , as intuitively expected. We now try to unveil the N dependence.

The function $\gamma_\phi = a/N$, with $a = 0.707$ yields a good fit. As can be seen in Fig. 4, the addition of a contribution $O(N^{-2})$ yields an excellent fit at large N :

$$\gamma_\phi = \frac{a}{N} + \frac{b}{N^2}, \quad (33)$$

with $a = 0.704$ and $b = 0.030$. We emphasize that other functional forms (such as different power laws) do not yield equally good results. We offer no explanation for the N -dependence in Eq. (33).

In Fig. 5 we show the N -dependence of the algebraic connectivity for a circle graph with equally distributed

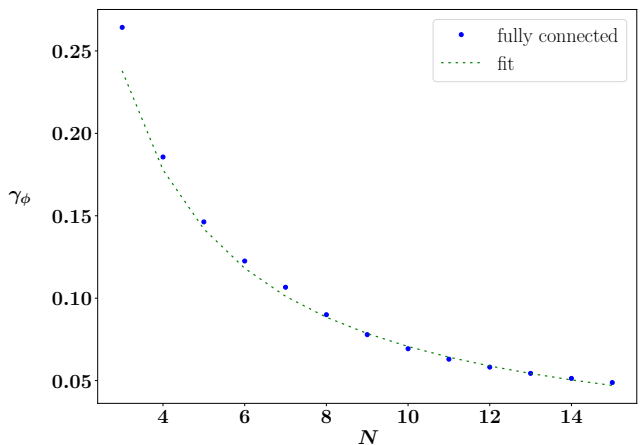


FIG. 4: Dots: algebraic connectivity. Dotted (green) line, fit in Eq. (33), with $a = 0.704$ and $b = 0.030$, obtained by fitting the points $N \geq 8$.

weights. This yields a good comparison with the data displayed in Figs. 3-4. The approach to equilibrium is much slower, as was to be, being the graph less connected. The best fit yields the functional dependence

$$\gamma_\phi = \frac{a}{N^{3/2}} + \frac{b}{N^{5/2}}, \quad (34)$$

with $a = 0.301$ and $b = -0.189 \times 10^{-3}$.

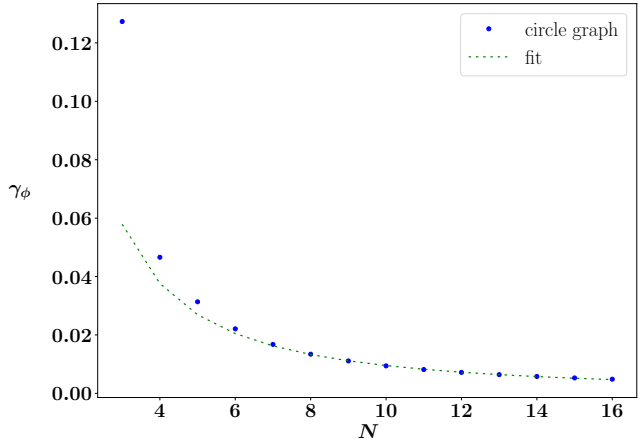


FIG. 5: Same as in Fig. 4, for the circle graph. Dots: algebraic connectivity. Dotted (green) line: fit in Eq. (34), with $a = 0.301$ and $b = -1.888 \times 10^{-4}$, obtained by fitting the points $N \geq 8$.

We now turn to an analysis of the convergence features of the network in the presence of noise. This will yield additional insight into the mechanisms of convergence and the bound (31).

In Fig. 6, we add a noise to the probabilistic weights in Eq. (32). Each probability is multiplied by a random number in the interval $[1 - \epsilon, 1 + \epsilon]$; the probabilities are subsequently normalized so that they sum up to 1.

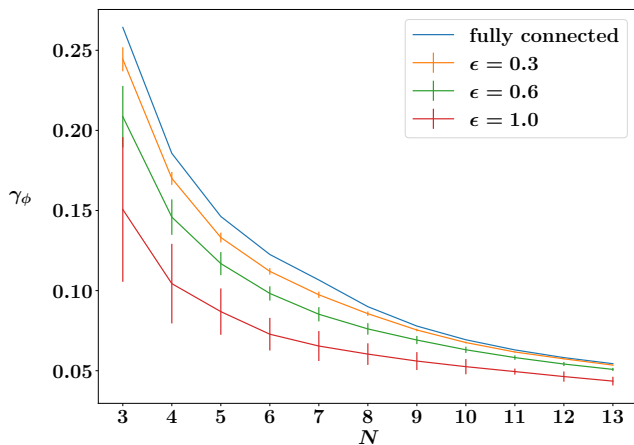


FIG. 6: Algebraic connectivity of a fully connected graph vs N , for different noise on the probabilistic weights p_{ij} . Noise ϵ increases from top to bottom. The vertical bars are standard deviations. The fits (not shown) always yield a dependence $\gamma_\phi = a/N + b/N^2$, with $(\epsilon = 0.3)$ $a = 0.695, b = -0.117$; $(\epsilon = 0.6)$ $a = 0.735, b = -1.013$; $(\epsilon = 1.0)$ $a = 0.702, b = -1.763$.

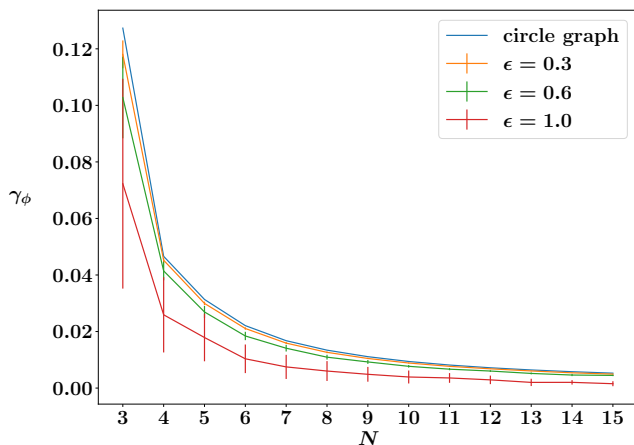


FIG. 7: Same as in Figure 6, for a circle graph. Noise ϵ increases from top to bottom. The vertical bars are standard deviations.

We take $\epsilon = 0.3, 0.6, 1$ (increasing noise), the last figure being the maximum value if the positivity of the probabilities is to be preserved. The presence of noise yields a slower approach to equilibrium. This result, at first a bit surprising, is understood by realizing that noise makes some probabilities smaller, so that some nodes are more isolated than others, and tend to equilibrate later. Notice that, at a given noise realization, the iterated map is always the same. Observe also that this behavior is in qualitative accord with the philosophy behind the bound (31).

In Fig. 7 we add a noise to the weights of a circle graph. As expected, in the light of the preceding comments, some nodes become more isolated than others, and the approach to equilibrium is significantly slower

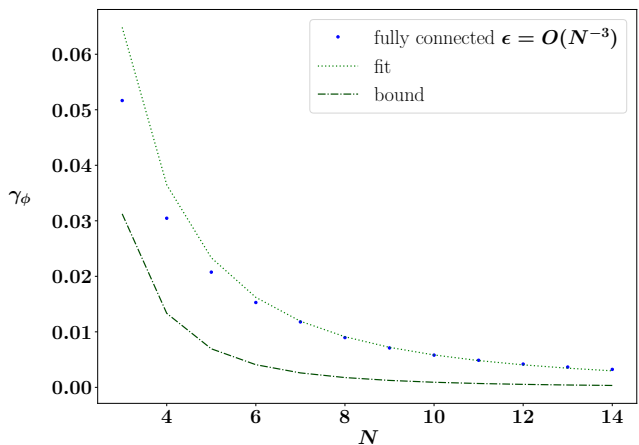


FIG. 8: A very unbalanced fully connected graph. $((N(N-1)-1)$ links have probabilities $\epsilon = O(N^{-3})$, while one link has probability $O(1)$. Dots: algebraic connectivity. Full (green) line: fit in Eq. (36), with $a = 0.629$ and $b = -3.831$, obtained by fitting the points $N \geq 8$. Dash-dotted (green) line: bound (31).

(as, unlike with the fully connected graph, is it now easier to create more isolated nodes). This corroborates and completes the picture discussed above.

One problem that remains to be understood is whether the bound (31) can be saturated in some sense. A moment's reflection shows that, in general, this cannot be the case. Indeed, take one of the $p_{ij} = 0$ in Eq. (31); the graph is almost fully connected (only one link is missing), but will nonetheless tend to equilibrium, as there are many nonvanishing links between any given qubit and the other qubits in the network. For such a graph, γ_ϕ must be strictly positive and β_* in Eq. (29) strictly smaller than 1.

Motivated by the preceding comments, in Fig. 8 we considered a fully connected network with very unbalanced weights: we took $((N(N-1)-1)$ links with probability $\epsilon = O(N^{-3})$, *except* one link with a probability $O(1)$, so that

$$\min_{ij \in I} p_{ij} = \frac{N^{-3}}{(1 + ((N(N-1)-1)N^{-3}))} \sim \frac{1}{N^3}. \quad (35)$$

As expected, in the light of the preceding comments and discussion, the approach to equilibrium is very slow (in fact, the slowest we have observed in our numerical simulations). However, as can be seen, the bound (31) is not saturated. A fit yields the dependence

$$\gamma_\phi = \frac{a}{N^2} + \frac{b}{N^4}, \quad (36)$$

with $a = 0.629$ and $b = -3.831$ (by fitting points with $N \geq 8$).

Summarizing, the numerical analysis shows that there are a number of factors that influence the approach to equilibrium in a fully connected quantum network

of qubits whose interactions are represented by CNOT gates. Change of connectivity and weights can induce very different convergence rates, even at the qualitative level. The mathematical bound (31) is clearly valid, but appears to be loose in most situations. Further analyses are required to elucidate the underlying equilibration mechanisms.

VII. CONCLUSIONS

We studied the rate of convergence of full graph quantum networks. Using analytic methods we gave estimates for this rate and by using numerical methods we determined the rates of convergence to the asymptotic state. The convergence is inversely proportional to the number of vertices-qubits forming the graph. The expansion coefficients have been determined numerically. The numerical tests are limited up to 15-16 qubits, which turn out to be sufficient to determine the convergence rates at leading order.

The estimate of convergence rates is clearly of fundamental importance, as it is one of the basic parameters characterizing random quantum networks. At the same time, the convergence rate is also of practical importance, as it gives experimental physicists the typical scale after which the network “equalizes” and its asymptotic is reached. As repeatedly mentioned, the determination of the asymptotics is in many cases accessible by analytic methods and can be worked out in detail. However, results (especially analytic ones) on the convergence rates are scarce. Our estimates, both analytic and numerical, are a step into this uncharted territory.

The observation in Sec. III enabled us to drastically simplify the problem, significantly reducing its complex-

ity. As already emphasized, besides such inherent complexity, a number of factors (connectivity, topology, probabilistic weights) heavily influence the approach to equilibrium, yielding very different convergence rates. While our work is limited to special types of graphs, we expect the approach and results to hold also for similar situations. Further work is needed in order to scrutinize the underlying equilibration mechanisms and possibly generalize the results discussed in this article to different networks.

Acknowledgements

SP would like to thank the Department of Physics of the Czech Technical University in Prague for their warm hospitality. The numerical analysis has been done on the CRESCO/ENEAGRID High Performance Computing infrastructure of ENEA. JN and IJ acknowledge the financial support from RVO14000 and “Centre for Advanced Applied Sciences”, Registry No. CZ.02.1.01/0.0/0.0/16 019/0000778, supported by the Operational Programme Research, Development and Education, co-financed by the European Structural and Investment Funds and the state budget of the Czech Republic and by the Czech Science foundation (GACR) project number 16-09824S. IJ was partially supported from GACR 17-00844S. SP acknowledges support by MIUR via PRIN 2017 (Progetto di Ricerca di Interesse Nazionale), project QUSHIP (2017SRNBRK), by INFN through the project “QUANTUM” and by Regione Puglia and QuantERA ERA-NET Cofund in Quantum Technologies (GA No. 731473), project PACE-IN. The work of AS is within the activities of the TQT, Trieste.

-
- [1] H. J. Kimble, *The quantum internet*, Nature **453**, 1023 (2008).
 - [2] B. Yurke, J. S. Denker, *Quantum network theory*, Phys. Rev. A **29**, 1419 (1984).
 - [3] G. Mahler, V.A. Weberruss, *Quantum Networks*, (Springer, Berlin, 1995).
 - [4] M. A. Nielsen, I. L. Chuang, *Quantum Computation and Quantum Information*, (Cambridge University Press, 2011).
 - [5] J. C. Maxwell, *On the Dynamical Theory of Gases*, Phil. Trans. Royal Society of London. **157**, 49 (1867).
 - [6] L. Boltzmann, *Ober die mechanische Bedeutung des zweiten Hauptsatzes der Warmetheorie*, Wiener Berichte **53**, 195 (1866).
 - [7] A.S. Holevo, *Statistical Structure of Quantum Theory* Lect. Not. Phys **61**, (Springer, Berlin, 2001).
 - [8] J. Novotný, G. Alber and I. Jex, J. Phys. A: Math. Theor. **42**, 282003 (2009). <https://doi.org/10.1088/1751-8113/42/28/282003>
 - [9] J. Novotný, G. Alber, and I. Jex, Cent. Eur. J. Phys. **8**, 1001 (2010).
 - [10] L. Boltzmann, *Studien über das Gleichgewicht der lebendigen Kraft zwischen bewegten*, Wiener Berichte **58**, 517 (1868).
 - [11] L. Boltzmann, *Weitere Studien ber das Wrmegleichgewicht unter Gasmoleklen*, Sitzungsberichte Akademie der Wissenschaften **66**, 275 (1872).
 - [12] S. Lorenzo, F. Ciccarello, and G. M. Palma, *Composite quantum collision models*, Phys. Rev. A **96**, 032107 (2017).
 - [13] M. Srednicki, *Chaos and quantum thermalization*, Phys. Rev. E **50**, 888 (1994).
 - [14] J. M. Deutsch, *Quantum statistical mechanics in a closed system*, Phys. Rev. A **43**(4), 2046 (1991).
 - [15] L. D’Alessio, Y. Kafri, A. Polkovnikov, and M. Rigol, *From quantum chaos and eigenstate thermalization to statistical mechanics and thermodynamics*, Advances in Physics **65**(3), 239 (2016).
 - [16] D. M. Basko, I. L. Aleiner, and B. L. Altshuler, *Metal-insulator transition in a weakly interacting many-electron system with localized single-particle states*, Annals of physics **321**, 1126 (2006).

- [17] A. Pal and D. A. Huse, *Many-body localization phase transition*, Phys. Rev. B **82**(17), 174411 (2010).
- [18] R. Nandkishore and D. A. Huse, *Many-body localization and thermalization in quantum statistical mechanics*, Annu. Rev. Condens. Matter Phys. **6**(1), 15 (2015).
- [19] M. Znidaric, T. Prosen, and P. Prelovsek, *Many-body localization in the Heisenberg XXZ magnet in a random field*, Phys. Rev. B **77**(6), 064426 (2008).
- [20] A. De Luca and A. Scardicchio, *Ergodicity breaking in a model showing many-body localization*, EPL (Europhysics Letters) **101**(3), 37003 (2013).
- [21] J.A. Kjäll, J.H. Bardarson, and F. Pollmann, *Many-body localization in a disordered quantum Ising chain*, Phys. Rev. Lett. **113**(10), 107204 (2014).
- [22] V. Ros, M. Müller, and A. Scardicchio, *Integrals of motion in the many-body localized phase*, Nuclear Physics B **891**, 420 (2015).
- [23] A. Aspect and M. Inguscio, *Anderson localization of ultracold atoms*, Phys. Today **62**(8), 30 (2009).
- [24] M. Schreiber, S.S. Hodgman, P. Bordia, H.P. Lüschen, M.H. Fischer, R. Vosk, E. Altman, U. Schneider, and I. Bloch, *Observation of many-body localization of interacting fermions in a quasirandom optical lattice*, Science **349**(6250), 842 (2015).
- [25] F. Arute, K. Arya, R. Babbush, D. Bacon, J.C. Bardin, R. Barends, R. Biswas, S. Boixo, F.G. Brandao, D.A. Buell, and B. Burkett, *Quantum supremacy using a programmable superconducting processor*, Nature **574**(7779), 505 (2019).
- [26] V.N. Smelyanskiy, K. Kechedzhi, S. Boixo, S.V. Isakov, H. Neven, and B. Altshuler, *Nonergodic delocalized states for efficient population transfer within a narrow band of the energy landscape*, Phys. Rev. X **10**(1), 011017 (2020).
- [27] G. Mossi and A. Scardicchio, *Ergodic and localized regions in quantum spin glasses on the Bethe lattice*, Philosophical Transactions of the Royal Society A: Mathematical, Physical and Engineering Sciences **375**, 20160424 (2018).
- [28] E.G. Rieffel, S. Hadfield, T. Hogg, S. Mandra, J. Marshall, G. Mossi, B. OGorman, E. Plamadeala, N.M. Tubman, D. Venturelli, and W. Vinci, *From Ansatzes to Z-gates: a NASA View of Quantum Computing*, Future Trends of HPC in a Disruptive Scenario **34**, 133 (2019).
- [29] M. Fiedler, *Algebraic connectivity of graphs*, Czech. Math. J. **23**(2), 298 (1973).
- [30] B. Mohar, *Eigenvalues, diameter, and mean distance in graphs*, Graphs and Combinatorics (**7**), 53 (1991).
- [31] A. Graham, *Nonnegative Matrices and Applicable Topics in Linear Algebra*, (John Wiley and Sons, New York, 1987).
- [32] F. R. K. Chung, *Spectral graph Theory*, (CBMS, American Mathematics Society, 1997).
- [33] B. Mohar, *The Laplacian spectrum of graphs*, (Wiley, New York, 1991).
- [34] N. M. M. de Abreu, *Old and new results on algebraic connectivity of graphs*, Lin. Alg. and its App. **423**, 53 (2007).
- [35] F. Iannone et al., *CRESCO ENEA HPC clusters: a working example of a multifabric GPFS Spectrum Scale layout*, Proceedings of the 2019 International Conference on High Performance Computing & Simulation (HPCS), 1051 (2019).
- [36] There are better bounds, but all of them depend on the graph parameters, whose determination is at least as difficult as the determination of the spectrum.
- [37] More precisely, two vertices can be connected only if they differ in the excitation of one qubit. Whether they are really connected then depends on the details of the interaction graph.